Precision manufacturing process monitoring with acoustic emission

D.E. Lee[a], I. Hwang[a], C.M.O. Valente[b], J.F.G. Oliveira[b], D.A. Dornfeld[a],*

[a]*Laboratory for Manufacturing Automation, Department of Mechanical Engineering, University of California, Berkeley, CA 94720-1740, USA*
[b]*University of Sao Paulo, Nucleus of Advanced Manufacturing, Sao Carlos, Brazil*

Abstract

Current demands in high-technology industries such as semiconductor, optics, MEMS, etc. have predicated the need for manufacturing processes that can fabricate increasingly smaller features reliably at very high tolerances. In situ monitoring systems that can be used to characterize, control, and improve the fabrication of these smaller features are therefore needed to meet increasing demands in precision and quality. This paper discusses the unique requirements of monitoring of precision manufacturing processes, and the suitability of acoustic emission (AE) as a monitoring technique at the precision scale. Details are then given on the use of AE sensor technology in the monitoring of precision manufacturing processes; grinding, chemical–mechanical planarization (CMP) and ultraprecision diamond turning in particular.
© 2005 Elsevier Ltd. All rights reserved.

Keywords: Acoustic emission; Precision; Process monitoring

1. Introduction

Current demands in high-technology industries such as semiconductor, optics, MEMS, etc. have predicated the need for manufacturing processes that can fabricate increasingly smaller features reliably at very high tolerances. This increasing demand for the ability to fabricate features at smaller length scales and at greater precision can be represented in the Taniguchi curve (Fig. 1), which demonstrates that the smallest achievable accuracy (and, as a consequence, smallest reproducible feature) decreases as a function of time [1].

In situ monitoring systems that can be used to characterize, control, and improve the fabrication of these smaller features are therefore needed to meet increasing demands in precision and quality. Sensor-based monitoring yields valuable information about the manufacturing process that can serve the dual purpose of process control and quality monitoring, and will ultimately be the part of any fully automated manufacturing environment. However, a high degree of confidence and reliability in characterizing

the manufacturing process is required for any sensor to be utilized as a monitoring tool. As demonstrated in a previous review paper by Dornfeld et al. [2], acoustic emission (AE) has demonstrated a high degree of confidence in characterizing various phenomena related to material removal, particularly at the microscale, hence lending credence to its suitability for precision manufacturing process monitoring. This work serves to demonstrate sensitivity of AE at the three different manufacturing regimes outlined in the Taniguchi curve; the normal/conventional, precision, and ultraprecision scales (Fig. 1).

2. Requirements for sensor technology at the precision scale

In material removal processes at the precision scale, the undeformed chip thickness can be on the order of a few microns or less, and can approach the nanoscale in some cases. At these length scales, the surface, subsurface, and edge condition of machined features and the fundamental mechanism for chip formation are much more intimately affected by the material properties and microstructure of the workpiece material, such as ductile/brittle behavior, crystallographic orientation of the material at the tool/chip interface, and microtopographical features such as voids, secondary phases, and interstitial particulates [3,4].

---

* Corresponding author. Tel.: +1 510 642 0906; fax: +1 510 643 7492.
E-mail addresses: cmov@sc.usp.br (C.M.O. Valente), dornfeld@me.berkeley.edu (D.A. Dornfeld).
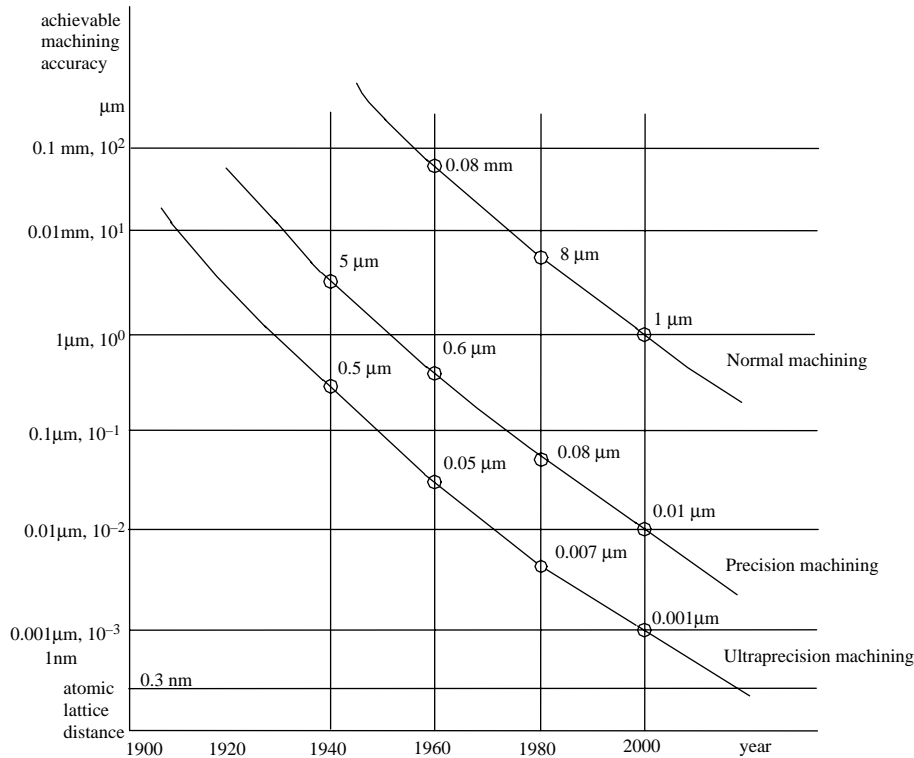
Fig. 1. Taniguchi curve [1].

Characterizing the surface, subsurface, and edge condition of machined features at the precision scale, as well as tracking relevant process parameters such as material removal rate (MRR), tool contact/cycle time, and state of tool condition (level of pad wear in chemical–mechanical planarization, wheel loading in grinding, tool wear in machining, for instance) are of increasing importance for monitoring, evaluating, and controlling the manufacturing process.

A great deal of work has been devoted to evaluating the applicability and need of sensors for a variety of manufacturing processes, with previous reviews by Dornfeld et al. [2,5] focusing on recent sensing techniques with respect to future manufacturing requirements. Likewise, an early review by Tlusty et al. examined the role of cutting force and AE as a means for condition monitoring and adaptive control [6], and Tonshoff et al. proposed techniques for condition monitoring strategies such as intelligent machining and multi-sensor systems [7]. One of the most comprehensive reviews of overall sensor technology and data processing techniques for automated machining was conducted by Byrne et al. [8]. Likewise, Iwata [9] surveyed the requirements of the Japanese machine tool industry for sensors and process monitoring. However, a key note in the above papers was their focus on monitoring at the conventional scale, and not necessarily at the precision or ultraprecision scales.

A variety of sensors (each having a degree of applicability depending on the level of precision required

or type of phenomena or control parameter that needs to be measured) are used to capture necessary information about the manufacturing process. Fig. 2, which serves as an update to a similar diagram from the aforementioned review paper [2], diagrams several different classes of sensors and their applicability to both level of precision (starting at the conventional scale and moving down the ordinate to ultraprecision material removal levels) and type of control parameter. It is important to note, however, that the boundaries for each sensor type are not necessarily 'hard' boundaries, and that continually improving sensor
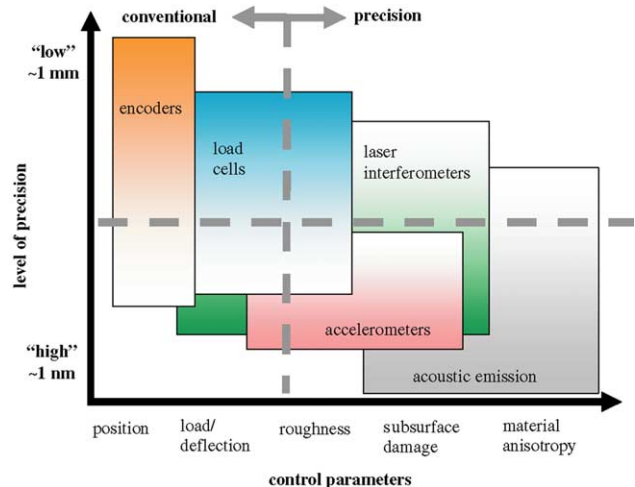

Fig. 2. Sensor application vs. level of precision and control parameters.

technology will allow sensors to cover a wider range of control parameters with increasing sensitivity (as of this writing, the recent introduction of microcutting load cells is a good example). Conventional measuring techniques such as load cells are suitable for measuring conventional-scale control parameters such as cutting and thrust forces at ranges from several to hundreds of Newtons. However, conventional sensors may not have the necessary signal-to-noise (*S/N*) ratio and sensitivity required to adequately and reliably characterize surface finish, subsurface damage, and cutting forces at the ultraprecision scale due to the extremely low cutting forces (~ 0.1 N and lower) and power consumption present in ultraprecision machining.

As illustrated in Fig. 2, AE is highly desirable due to its relatively superior *S/N* ratio and sensitivity at the ultra-precision scale when compared to conventional load cell technology, with different levels of AE detectable even at extremely low depths of cut [4]. This is true even when the chip formation process diminishes and the only remaining tool–material interaction involves rubbing and burnishing of the surface along different grain orientations. Another particular advantage of AE is that it tends to propagate at frequencies (typically the kHz/MHz range) well above the characteristic frequencies attributed to machining (such as spindle RPM) or natural structural modes in the machine tool structural loop, minimizing the introduction of noise into the AE signal from the above phenomena. Hence, AE is particularly well-suited because of its ability to detect microscale deformation mechanisms within a relatively 'noisy' machining environment.

3. Sources for AE in precision manufacturing

Machinists have long used audible feedback during machining as a means of monitoring the cutting process, with skilled machinists able to judge even minute variation in tool wear and surface finish simply by listening to the machining process. The unique sound given by metals during plastic deformation is nothing new, with the unique 'tin cry' sound given by tin being plastically deformed as a common one. The above examples all share the common trait of the generation of elastic stress waves within a medium due to plastic deformation. The term *acoustic emission* typically refers to elastic wave propagation in the ultrasonic frequency range (~ 20–2000 kHz). Unlike ultrasonic non-destructive techniques (NDT), which are a means of active scanning (ie. generation, transmission, and collection of signal), acoustic emission is mostly a passive means of scanning, much akin to holding a microphone or other sensor and 'listening' for various phenomena.

Since plastic deformation is a strong source of AE, material deformation-based manufacturing processes have the most potential for acoustic emission-based monitoring. Some of the earliest work on examining the source of AE

in plastic deformation was conducted by Fisher and Lally [10], who found sharp drops in flow stress during uniaxial loading of single crystal metals and attributed these drops to the propagation of localized deformation bands (possibly slip bands) in the crystal. The formation of these bands were believed to be due to the near simultaneous movement of a large number of dislocations, upon which stress relaxation waves were released and subsequently detected as AE. Since then, a great deal of research has been performed on identifying sources of AE in manufacturing processes, with Moriwaki [11] conducting a comprehensive review of AE sources in machining. Fracture was identified as one possible source, as the propagation of microcracks releases elastic energy due to the generation of new surfaces. Friction or rubbing between two surfaces (such as at the tool/chip interface) is another potential source; surface asperities come into contact and are plastically deformed, and possibly even welded together. As the surfaces slide over one another, these asperities are deformed further and even fractured, hence generating AE.

In precision machining, AE can be attributed to several sources at the tool/chip interface (shown in Fig. 3). At the tool/chip interface in conventional machining, AE is typically generated in the primary shear zone (shear region ahead of the tool), secondary shear zone (region of contact between tool and chip), and the tertiary shear zone (contact between the machined surface and flank). While at the conventional machining scale where the DOC is typically on the order of tens of microns and higher, AE is largely due to rubbing and friction at the tool/chip interface, including both the secondary and tertiary shear zones. At the precision scale and below, however, it is believed that the majority of AE signal generation is generated through the interaction of the tool tip with microstructural features of the workpiece, such as voids, inclusions, grain boundaries, and bulk dislocation interactions in the shear zone (see Fig. 3).

Several studies have focused on the effect of various machining parameters on the resultant AE signal. Liu established a good match between modeled and experimental AE root-mean-square (RMS) signal for diamond turning, and found a strong correlation between chip thickness, cutting speed, and AE RMS [12]. Likewise, further work by Chen established an exponential decrease in specific AE RMS (analogous to specific cutting energy, energy density, or energy/chip volume) vs. chip thickness [13]. AE sensitivity down to chip thicknesses of 0.01 μm was found, with a sharp difference in specific AE RMS between worn and sharp tools. The increase in specific cutting energy with decreasing chip thickness and tool wear was believed to be due to the ratio of tool edge radius to uncut chip thickness; as the uncut chip thickness decreases below the edge radius of the tool, a transition in the cutting mechanism takes place where an effective negative rake angle is established, which shifts the cutting mode to a more
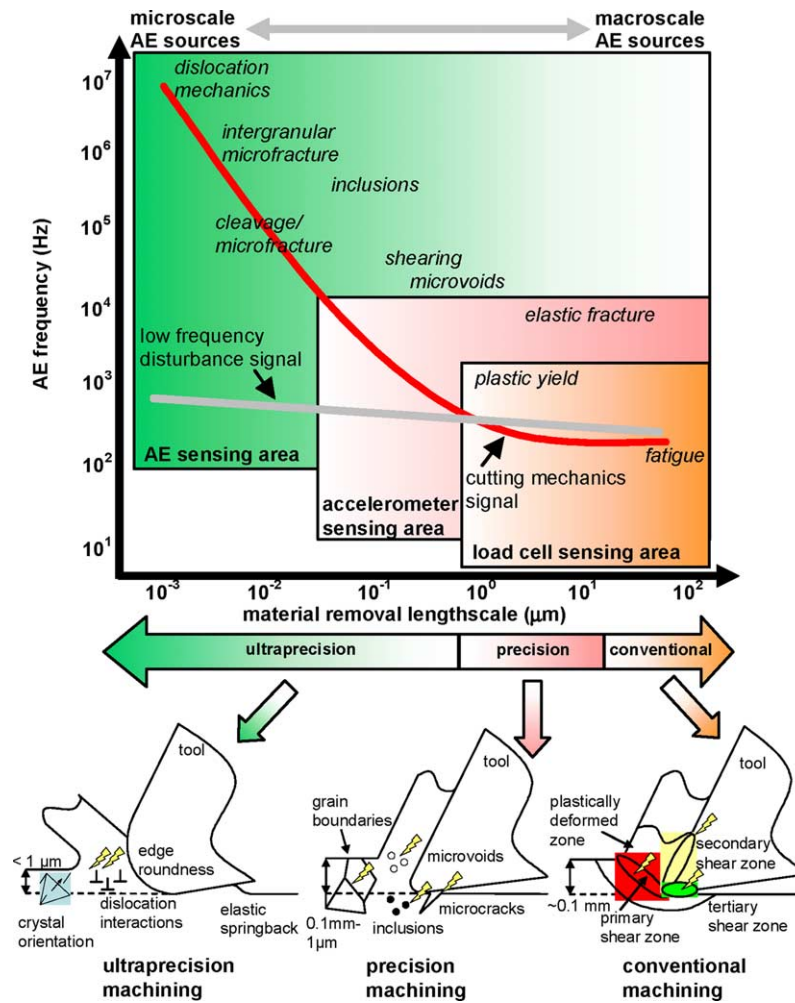
Fig. 3. Sources of AE at varying stages of material removal.

energy-consuming one dominated by rubbing and burnishing. This effective negative rake angle also helps explain the increase in specific cutting energy for worn tools, as worn tools have a larger edge radius and require more energy than sharp tools to initiate chip formation.

4. AE-based monitoring of grinding wheel dressing

Currently, a conventional grinding process requires a complex sequence of tasks in order to start production on a workpiece, including equipment setup, machining of initial test samples, calibration of the tool, and frequent control and correction of the process parameters. AE can serve as a means for the complete automation of all these steps [14]. However, in grinding, the two main limitations of AE-based monitoring solutions are the oscillation of the RMS level and signal saturation. Despite these limitations, AE can be very effective for contact detection between moving surfaces. The following section will focus on a Fast AE RMS analysis and mapping technique for wheel condition monitoring in grinding.

4.1. Fast AE RMS analysis for wheel condition monitoring

A new method for process monitoring based on short-term analysis of AE RMS patterns is proposed. Since AE RMS changes occur after a considerable period of time, the short time evaluation could be a solution for a reliable AE application. Fig. 4 shows a proposed system where the acoustic emission obtained from the contact between diamond tool and grinding wheel (or grinding wheel and workpiece in grinding monitoring) is converted to an RMS level and acquired by the computer by using an A/D conversion board [14]. The sampling rate range varies from 60 to 500 kHz, depending on the chosen resolution in the circumferential direction. A sampling rate of 2 kHz was used in this particular case to map each rotation of the grinding wheel, which corresponds to a resolution of about 0.5 mm/sample. To be able to measure the contact of the diamond tool with each abrasive grain, the RMS calculation must be performed using a very fast time constant. The time constant was calculated as the average time spent for two consecutive hits between abrasive grains and the diamond tool. This calculation was done for a 60
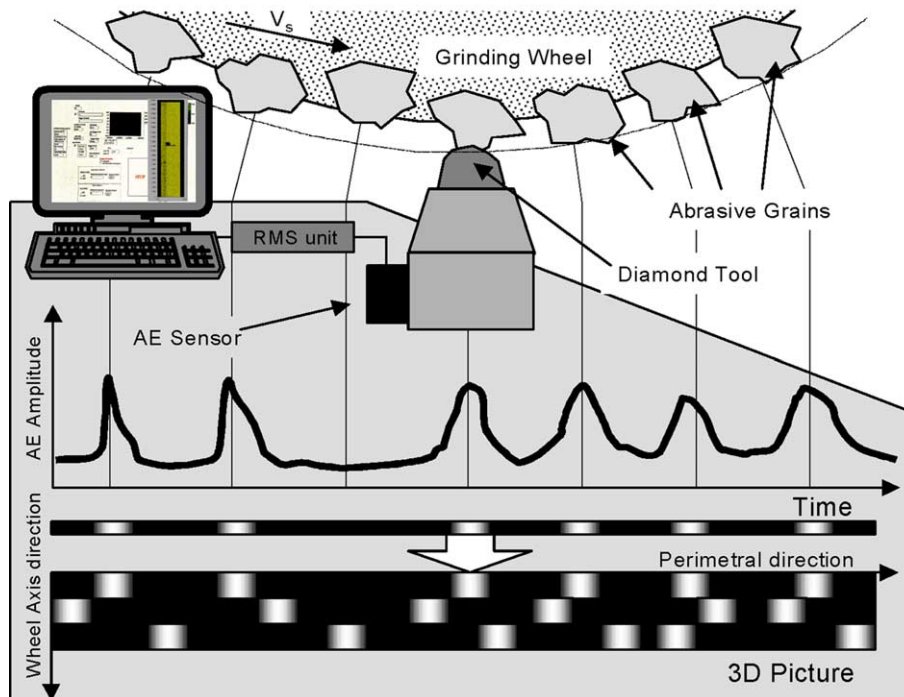
Fig. 4. Procedure for AE signal graphical mapping construction.

mesh, L-structure aluminum oxide wheel. The average distance between grains measured was about 0.38 mm with a grinding speed of 45 m/s, so a time constant of 10 ms was found.

In AE signal processing, the RMS calculation is normally done after having the raw signal filtered. Due to the very small time constant used in the RMS calculation, it was established that a high pass filter with a cut-off frequency of 100 kHz be used. A specific AE signal processing unit has been developed for this system. The data acquisition is made in data groups where each one-dimension array of data corresponds to a full rotation of the grinding wheel. The AE signal acquisition starts in each rotation triggered by a magnetic sensor positioned in the wheel hub where a reference pin is installed. A graphical mapping of the AE signal with a color intensity scale is then created. During the wheel dressing operation, the mapping is constructed in real time by adding columns in the array as the dresser travels along the wheel surface.

The system can be used for different evaluation procedures, including

Dressing evaluation. During the dressing operation, the interaction between dresser and grinding wheel can be acoustically mapped. Lack of contact between dressing tool and grinding wheel will appear as dark areas in the map.

Topographic mapping. In this case the map is similar to that obtained for the dressing operation but using the dressing depth of cut nearly zero or with a value close to the undeformed chip thickness for the operation. In this case the map shows the active surface of the grinding wheel, which means the surface that will actually be in contact with the workpiece during grinding.

Grinding evaluation. During a plunge grinding operation the interaction between the grinding wheel and the workpiece can be evaluated. In this case a different map is obtained where one axis is the grinding time and the other shows the average acoustic energy in the whole wheel length along its perimeter.

4.2. Grinding wheel topographical mapping

Fig. 5 shows an output from the acoustic mapping system when used during a topographic mapping procedure. The vertical and horizontal directions are the wheel perimeter and width, respectively, with a spatial resolution of 2 samples/mm. The depth of interaction between diamond tool and grinding wheel used was 1 μm (in the range of elastic contact). The color intensity shows the acoustic emission RMS value measured from the interaction between dressing tool and the abrasive grains. Darker areas correspond to lower acoustic energy detected by the sensor. The L-shaped mark was created in the wheel surface in order to evaluate the system performance. Dark areas show worn regions of the wheel where the dressing tool had lower interaction with the abrasive grains. The main vertical worn band on the left side was a result from a grinding operation made with the workpiece shown in the photo of Fig. 8a. In this figure, the 'L' mark produced on the wheel surface and a magnified view of its representation in the AE graphical mapping is shown.
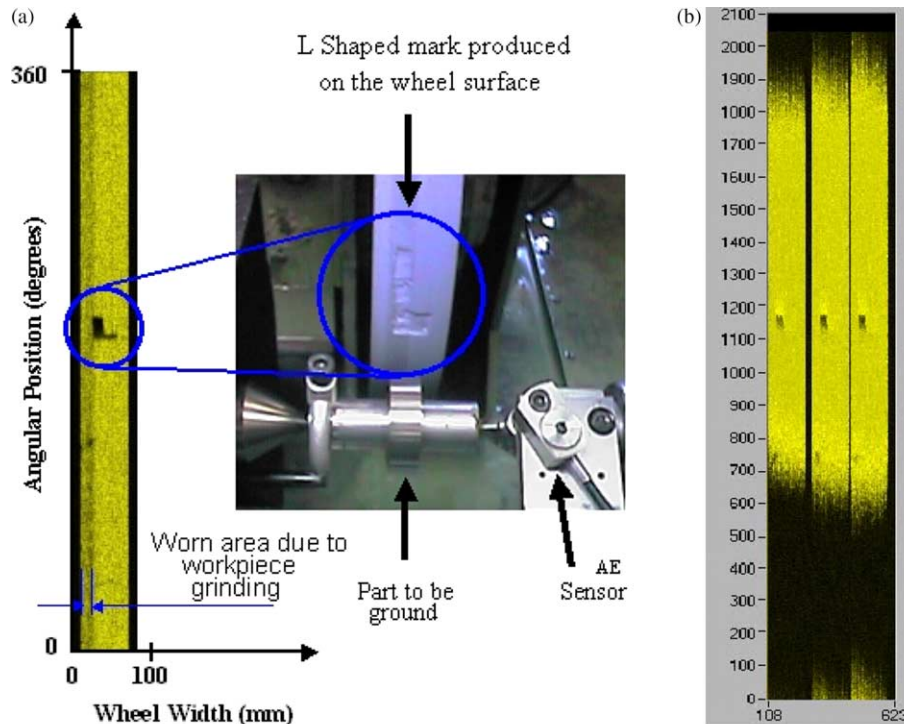
Fig. 5. (a) L-shaped mark produced on the wheel surface with corresponding AE map during dressing. (b) Dressing of unbalanced grinding wheel (first three strokes, 2 μm per pass).

It was observed that the AE mapping system could generate an image similar to the surface topography present on the grinding wheel surface, even using a very small depth of interaction with the diamond tool. A spark-out dressing was also tested (depth of interaction = 0) and the result was nearly the same. The use of equal depth of interactions may lead to reading error in the case of any thermal deformation in the machine structure.

The same grinding wheel was dressed in order to remove the damage produced by the grinding operation. The dressing depth of cut was 2 μm per pass. This small value was chosen in order to evaluate the depth of the damage produced by the grinding operation. The maps of three consecutive dressing strokes made in an unbalanced grinding wheel are shown in Fig. 5b. The wheel was dressed and then unbalanced using an automatic balancing system in manual mode. Each dressing operation was performed with a dressing in-feed of 1 μm. After six dressing strokes, the grinding wheel eccentricity disappeared, and the real unbalancing displacement level was calculated to be about 6 μm. The unbalancing device installed in the machine demonstrated a vibrational amplitude of only 1 μm (corresponding to the green zone for grinding). This strong difference is caused by the fact that the vibration sensor measures the vibration amplitude in the machine bearings while the acoustic mapping system measures the actual wheel eccentricity caused by the lack of balancing. The sequence shows exactly the position of the heavier side of the grinding wheel and the reduction in the

eccentricity after dressing. This is another important piece of information provided by the mapping system, since most balancing devices for grinding machine use vibration sensors as feedback. It was observed that the minimum vibration level does not lead to the best concentricity of the grinding wheel. Therefore, the information provided by the mapping system could be used as a feedback signal when balancing CBN wheels during touch dressing operations where this problem is more critical [14].

4.3. Wheel wear mechanism

Fig. 6 presents two experiments to demonstrate the influence of the wheel wear behavior in the AE map. Each stripe in the graph represents a single grinding cycle or a single workpiece in a production line of automotive components. The workpiece material was Inconel and the grinding wheel is a very hard grade, low friability aluminum oxide specification (DA 80 R V). The second experiment was a plunge grinding operation of hardened AISI 4340 steel using a soft white aluminum oxide grinding wheel (AA 60 G V).

The image composition of the several mappings in Fig. 6 shows two distinct types of wheel wear behavior. In the first experiment the consistent pattern around the wheel shows that it is not losing grains. In the second experiment, the transformation indicates that the wheel is indeed losing grains. These results were confirmed by checking the workpiece size plot (stable for the first case and an
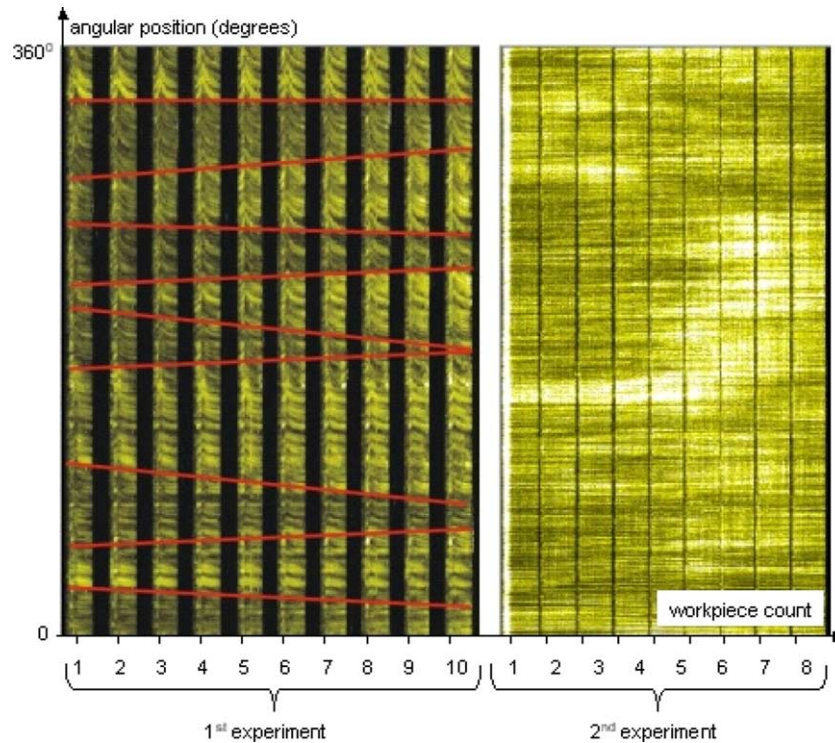
Fig. 6. Mapping of AE from a grinding process showing two types of wear mechanisms.

increasing tendency in the second case), workpiece temperature (grows for the first experiment and constant for the second) and power plots (power grows in the first experiment and remains constant for the second one) [14].

5. AE-based monitoring of face milling

The fast AE RMS graphic mapping system used for the AE monitoring work for grinding was also used to monitor a face milling process. Previous work by Diei and Dornfeld established a high degree of sensitivity of the AE signal to the individual chip formation mechanism in face milling, with a significant variation observed in the AE signal (processed through time-difference signal processing techniques) with respect to different stages of the chip formation process, with significant increase in AE signal observed upon the initiation of chip formation (due to initial impact of the insert with the workpiece) and exit of the insert from the workpiece [15,16] (see Fig. 7a).

In the face milling monitoring work, a ROMI Discovery 3-axis CNC milling center was used with an AE sensor attached directly to the workpiece [17]. The AE RMS signal was collected during a typical machining operation (6 insert cutter, 200 RPM, 0.1 mm/insert feed, 0.2 μm axial DOC) in a continuous fashion similar to the techniques and DAQ system parameters used in the grinding monitoring technique. Each vertical data trace in the AE RMS intensity mapping in Fig. 7b corresponds to one spindle rotation, with a clear spike in AE signal occurring due to the initial impact

of the insert with the workpiece (similar to that seen in Fig. 7a). Successive spindle rotations are shown along the horizontal axis, for a total of approximately 200 total revolutions in the intensity mapping. The AE RMS signal for each cutting insert can be clearly seen (numbered 1–6) with a separation of 60 degrees between inserts. After several tens of spindle revolutions, AE signal due to the rubbing of inserts on the trailing edge of the cutter can be observed, although the AE signal due to rubbing of inserts 2 and 6 can barely be seen (see Fig. 7b). This AE mapping technique serves as a means for tool condition monitoring in face milling, particularly for tool contact, breakage, and insert positional precision within the cutter [17].

6. AE-based monitoring of chemical–mechanical planarization

Chemical–mechanical planarization (CMP) is one of the key enabling technologies in the semiconductor manufacturing industry today for the fabrication of extremely smooth and flat surfaces on a variety of semiconductor substrate materials. In order to meet the requirements of current lithography tools which require extremely stringent tolerances for flatness and planarity, CMP is capable of planarizing a 300 mm (current industry standard) diameter wafer achieving surface roughness on the order of 1–2 nm R_a and global planarity well below 0.5 μm. However, CMP has also become one of the key bottleneck or roadblock issues in semiconductor manufacturing today [18].
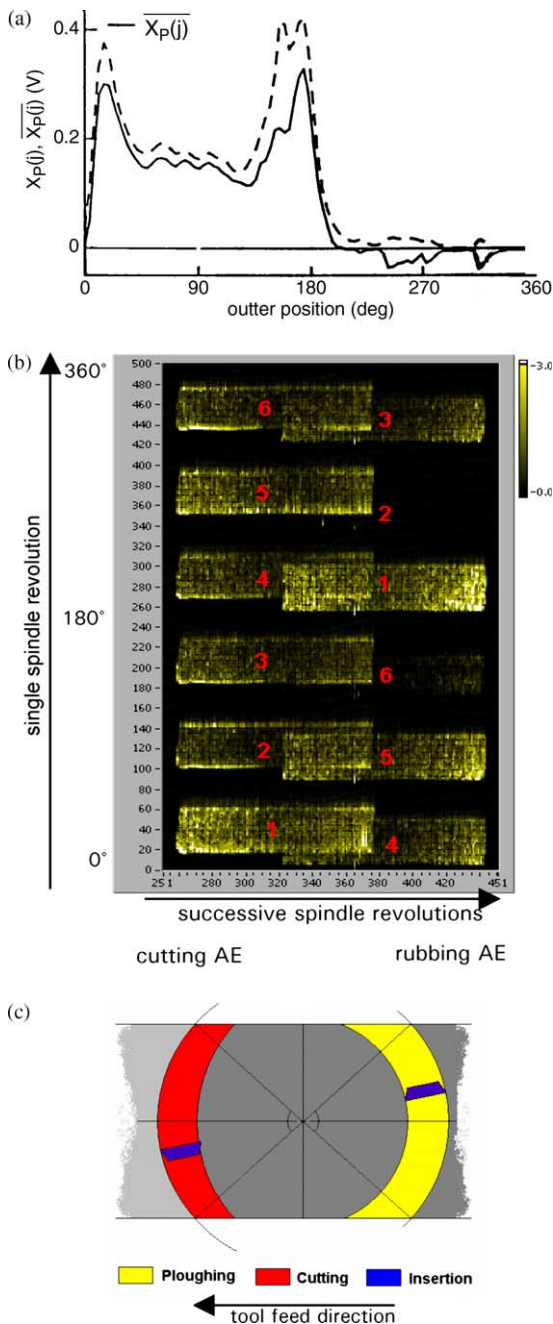
Fig. 7. (a) AE response for single chip formation in face milling. (b) AE map for face milling operation. (c) Tool motion relative to workpiece.

The decreasing line widths of semiconductor devices require new materials, such as copper and the so-called low-k dielectrics, which further challenge the process. Preferential polishing rates of adjacent materials, or surface features resulting from previous manufacturing steps, often lead to defects such as dishing which frustrate efforts to obtain planarity. The abrasive slurry can also induce defects such as surface contamination, scratches, slurry residue, etc. hence predicating the need for a reliable means of monitoring the CMP process.

6.1. Precision scribing of CMP-treated wafers

As a means of investigating the process physics of CMP, and to further evaluate the sensitivity of AE to the material removal physics taking place, a series of scribing tests on a CMP-processed oxide wafer were conducted [19]. In the CMP process for oxide planarization, the bulk of material removal takes place on a 'chemically weakened' layer consisting of a highly hydrated and loosely bound network of silica on the order of a few nanometers in thickness (see Fig. 8). The second layer is a 'plastically compressed layer' around 20 nm deep from the chemically weakened layer, depending on process conditions. Unlike the chemically weakened layer, this layer is represented by a plastically compressed network of silica that has higher density. A bulk layer also exists below the plastically compressed layer that is not affected by the CMP process. Because of the variation in the material properties of each layer, it was initially postulated that the AE RMS signal obtained during material removal of these distinct layers would differ.

In order to assess the mechanical properties of the oxide layer, a scribing operation using a single point diamond turning machine was used (see Fig. 9). The setup involved mounting a polished oxide wafer at a slight angle of $\sim 2°$ and scribing across surface, with the tool engaging with an increasing depth-of-cut (DOC) as the tool traversed over the surface. An AE sensor was attached to the front side of the wafer and used to monitor these scratch tests.

During the scribing operation, two transitions (one from the chemically weakened layer to the plastically compressed layer, and the other from the plastically compressed layer to the bulk) appear as distinct features in the AE RMS signal. Fig. 10 shows the AE signals from the scratch test of
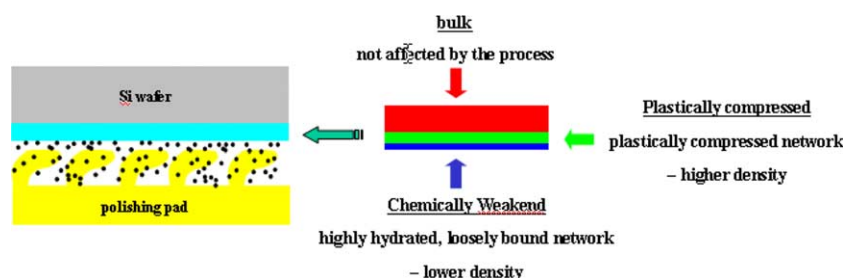

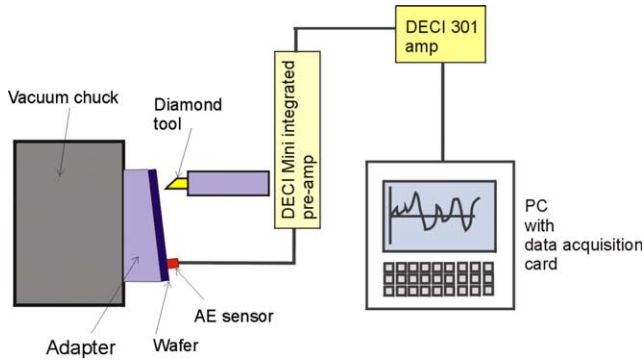Fig. 8. Three distinct layers exhibited in oxide CMP.

Fig. 9. Experimental setup for CMP oxide wafer scribing operation.

post-CMP wafers. As postulated, the variation in the AE signal reflects the three distinct layers and the transitions from one layer to another. The first part in Fig. 10 shows an 'air-cut' region where the tip is disengaged from the chemically weakened layer, and the very onset of contact between the tool and wafer. Since the chemically weakened layer consists of a loosely bound network of silica and is only a few nanometre deep, the AE RMS signal from this layer differs only slightly from that of the air-cut region. As the tip starts to touch the wafer, within 10 ms, the AE signals burst and increase over time for about 70 ms, which corresponds to a DOC of 30 nm, and confirms that the plastically compressed layer was engaged at this time. Beyond this part, the AE signals monotonically increase, without significant deviation or burst signal, meaning that the tool is cutting in the bulk layer of the oxide.

6.2. AE-based endpoint detection for CMP

In semiconductor manufacturing, the use of CMP in thin-film polishing for a fixed time is commonly used. However, due to fluctuations in the process, such as material-removal-rate (MRR) inconsistency, pad degradation, and

non-uniformity issues, over- or under-polishing can occur. An endpoint detection system is required to insure that only the desired thickness of material is polished during the CMP process, thus offering many manufacturing advantages such as improved process yields, closer conformance to target requirements, and higher throughput.

In order to evaluate the feasibility of AE as an in situ endpoint detection technique, two different sets of wafers were polished with a desktop CMP machine. The first set of wafers consisted of stacked films of oxide (5000 Å) at the bottom, tantalum (5000 Å) in the middle, and copper (1500 Å) at the top as an example of the copper damascene process. The wafer was polished with a conventional IC 1000 polyurethane pad and alumina-based slurry with 2.5% H_2O_2. The second set of wafers consisted of film stacks ranging from oxide (2000 Å) at the bottom to nitride (1000 Å) at the top, representing a shallow trench isolation process, and was polished with fixed abrasives and pH-adjusted deionized water (pH = 11.5). During the CMP process, both AE signals and frictional force data were collected with a DAQ system, and the experimental data for the copper damascene test wafers are plotted vs. time in Fig. 11a.

The endpoint was triggered at the edge of the wafer where copper was first cleared because of higher material removal at the edge. The phenomenon of the edge of the wafer clearing first also occurred in the second polishing step that removes the remaining copper and barrier layer. As shown in Fig. 11a, AE RMS signals clearly show the transition from tantalum to oxide, indicating the ideal endpoint whereas frictional force signals constantly increase as polishing time continues, making it difficult to detect the desired endpoint with frictional force alone. A similar trend was also observed for the STI test wafers during polishing, with a very sharp transition observed in the AE RMS signal when the oxide completely cleared (see Fig. 11b). These transitions are believed to be directly related to the variation
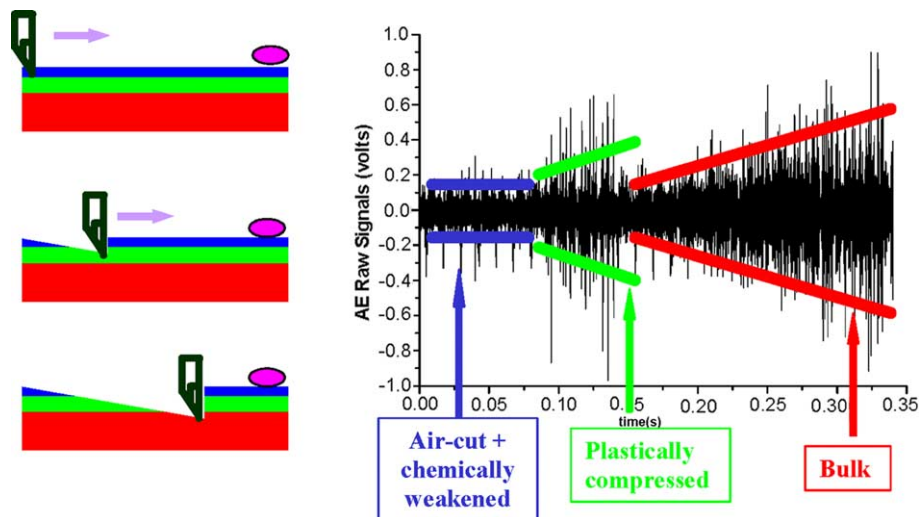

Fig. 10. Variation in AE RMS signal during scribing of CMP-treated oxide wafer.
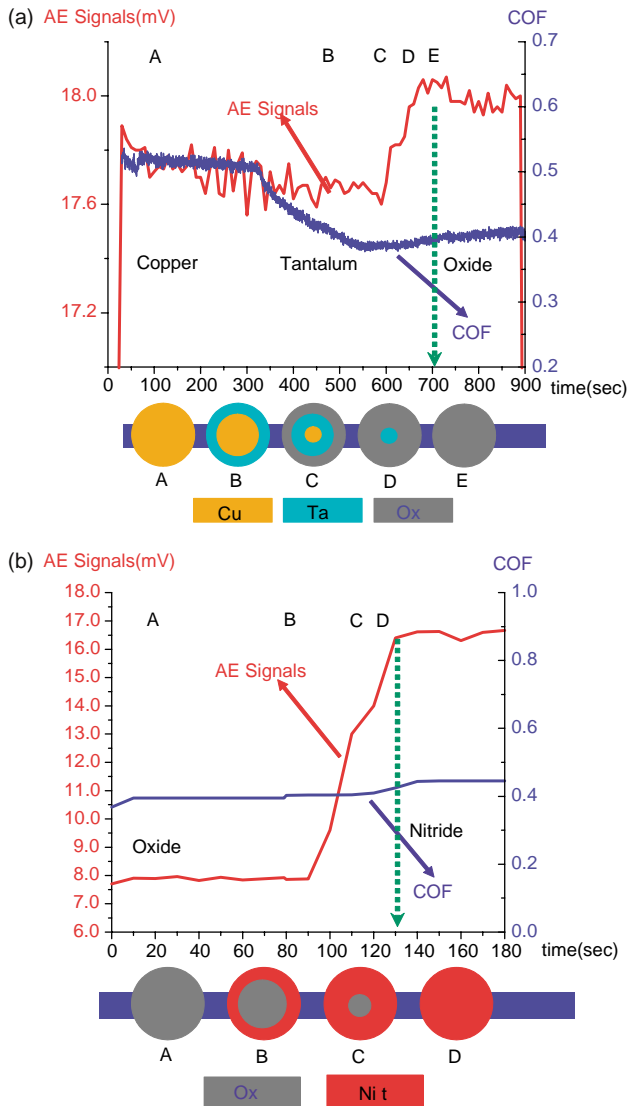
Fig. 11. AE RMS endpoint detection for (a) Cu damascene CMP process. (b) STI CMP process.

in material properties of each of the films, with harder materials (such as nitride) demonstrating an increase in AE RMS signal during polishing due to the increase in energy required to initial material removal, whereas less-hard materials such as copper exhibit lower AE RMS signal during polishing [19]. However, the frictional force does not exhibit the same sharp transition as the AE RMS signal, demonstrating the superior *S/N* ratio of AE for the material removal process in CMP when compared to frictional force.

7. AE-based monitoring of ultraprecision machining

7.1. Monitoring of precision scribing

To examine the effect of crystallographic orientation during ultraprecision machining, a series of nearly-parallel slow-speed scribes on the surface of an oxygen-free high-conductivity (OFHC) polycrystalline copper workpiece (250 μm average grain size) was taken. A 0.274 mm nose radius single crystal diamond tool was chosen as the tool of choice since the tool tip was considerably smaller than the average grain size of the workpiece. The workpieces were clamped onto the spindle of the lathe, and the spindle was rotated alternately and locked to allow for slow-speed scratches. A scratch speed of 0.7 mm/sec was used, and the infeed (depth of cut/DOC) setting was set at a constant value of 10 μm throughout the experiment. After each scribe, the spindle was unlocked and rotated slightly ($\sim$1 degree) to produce a radial pattern of scribes (although the scribe pattern can be approximated as a raster scanning pattern over this small angle of rotation). A similar DAQ system to that shown in Fig. 11 was used, with both cutting force and AE RMS signal collected during each scribing operation.

After collecting data from a series of scribes (typically on the order of 15 quasi-raster pattern scribes), the data was reduced, and a color intensity mapping function in MATLAB was used to plot the cutting force and AE signal as a function of position, with the color map representing the respective magnitude of the signal. Fig. 12 shows a graphical representation of the cutting force and AE RMS signal for a series of 15 scratches, along with a micrograph of the workpiece surface before scratching. Fig. 13 shows the cutting force and AE RMS for the 5th scribe.

Both the cutting force and AE RMS signal reproduce a crude representation of the grain structure of the material. The variation in force and AE RMS signal is largely due to the fact that each grain has a particular crystallographic orientation, so as the tool passes from one grain to another, a new slip system in the grain is being activated, which changes the amount of applied stress (and cutting force) required to initiate deformation. If the cutting speed and tool cross-section are constant, then the AE RMS is simply proportional to the energy (and cutting force) required to initiate deformation. The activation of different slip systems as a function of grain orientation causes the energy of the resulting AE RMS signal to fluctuate accordingly. Of particular note is the good match found between the mappings for the force and AE RMS signal, indicating that advances in load cell technology can allow for improved sensitivity to process mechanisms at the precision scale.

7.2. Monitoring of ultraprecision turning of single crystal copper

The sensitivity of AE to crystallographic orientation was also tested for single crystal materials. Fig. 14 shows a sample trace of AE RMS data for a single revolution of cutting on a <100> workpiece. An approximate sinusoidal variation in AE RMS can be seen in this data set. Each trace of AE RMS data is then collected in a data array in
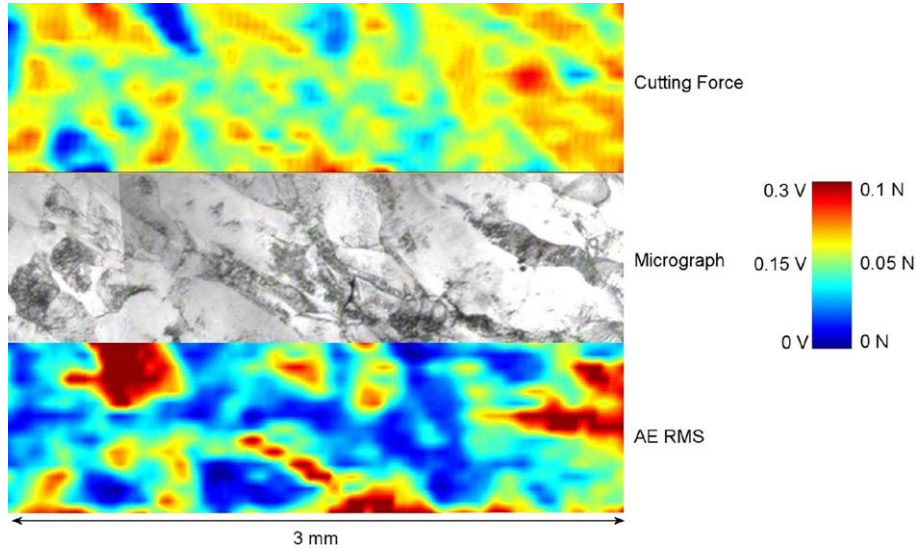
Fig. 12. Force/AE response for 'quasi-raster' scratch pattern.

LABVIEW, and is represented graphically as an intensity plot in Fig. 16. This intensity plot shows AE RMS signal as a function of spindle revolution, with subsequent traces of data for each spindle revolution progressing from left to right for a total of about 80 revolutions for a single face turning pass of the single crystal workpieces. Signal intensity or voltage levels are plotted according to a color intensity map, with a black color corresponding to zero signal, signal saturation at 3.5 V corresponding to a white color, and intermediate signal values appearing as shades of gray.

A Cartesian-polar transform allows for the data in Fig. 14 to be replotted on a polar intensity map as shown in Fig. 15a. In the polar intensity map, the AE RMS voltage is plotted vs. physical position on the workpiece, giving an indication of the variation of cutting energy as a function of crystallographic orientation. Fig. 15b and c show the theoretical variation in Taylor factor for a <100> crystal as a function of orientation, and an image of the chemically etched surface of the <100> workpiece after machining, respectively. A good correlation can be seen between the theoretical and experimental polar mappings, and variation in the surface finish of the chemically etched workpiece.

Fig. 16 shows SEM images of the machined surface before chemical etching. Fig. 16a shows the surface corresponding to areas that demonstrated low AE RMS signal levels of approximately 0.5 V, and Fig. 16b shows the surface of areas with AE RMS values of approximately 2 V. Dornfeld et al. postulated that this variation in AE signal corresponded to the variation in the orientation-dependent Taylor factor (representative of the yield stress, and consequently, specific energy required to initiate plastic deformation in a single crystal material) of the workpiece [20]. These regions of high and low AE RMS signal
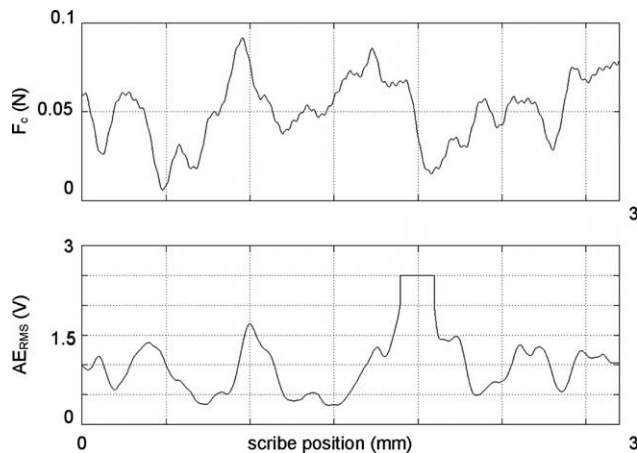

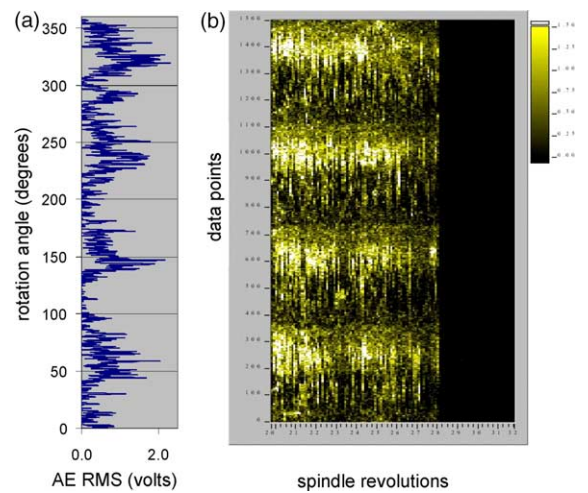Fig. 13. Individual force/AE response for single scribe (5th scribe).

Fig. 14. (a) AE RMS data trace for single revolution of face turning of <100> workpiece. (b) Cartesian intensity plot of AE RMS data for face turning.
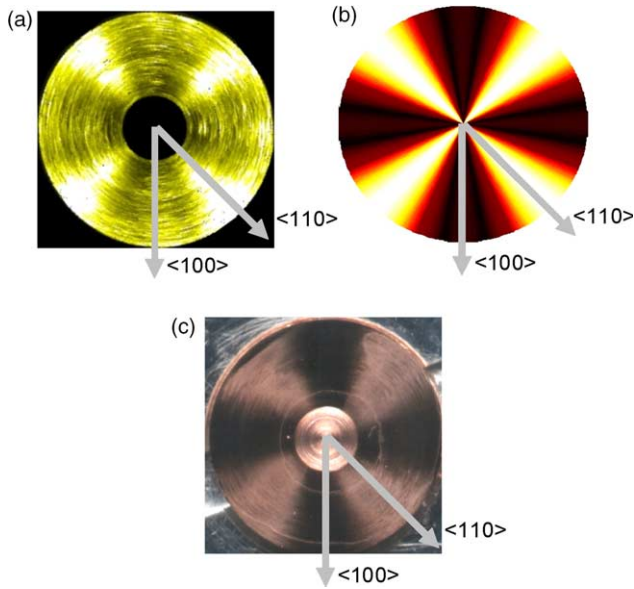
Fig. 15. (a) Experimental AE RMS polar map for <100> workpiece. (b) Taylor factor-based theoretical AE RMS polar map for <100> workpiece. (c) Chemically etched surface of <100> workpiece after machining.

correspond to regions that demonstrate high and low Taylor factors (ranging from 2.4 to 3.7), respectively. Crystallographic orientations that have a relatively high Taylor factor yield machined surfaces that are significantly rougher than areas with a relatively low Taylor factor. Fig. 16c shows a relatively smooth surface finish of 42.4 nm R_a (measured with a Wyko surface interferometer) while Fig. 16d shows the rougher surface with a surface finish of 75.6 nm R_a.

7.3. Monitoring of ultraprecision turning of polycrystalline copper

Fig. 17a shows an AE polar map for a polycrystalline OFHC copper workpiece. Although this piece was supposed to have an average grain diameter of 250 μm, several large grains were still observed on the workpiece. The AE polar map in Fig. 17a shows good correlation with the chemically etched workpiece surface, shown in Fig. 17b. While small grains below 100 μm cannot be resolved in the AE polar map due to DAQ limitations, the larger grains appear very clearly in both the chemically etched surface and AE polar map. Because these large grains can serve as defects that affect the homogeneity of the surface finish, the AE polar mapping technique, in addition to serving as a tool contact sensor, provides a very convenient means of detecting potential trouble spots or defective areas on the workpiece
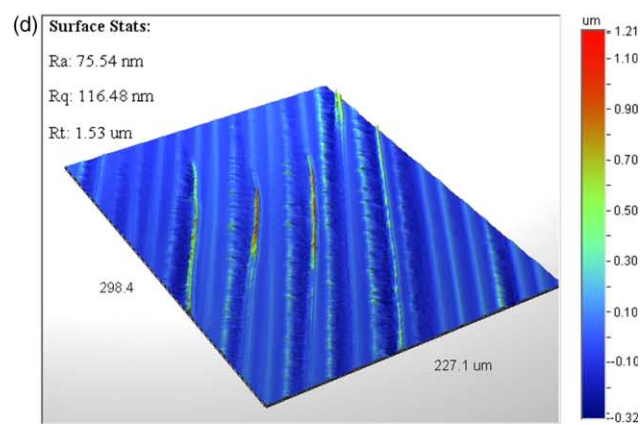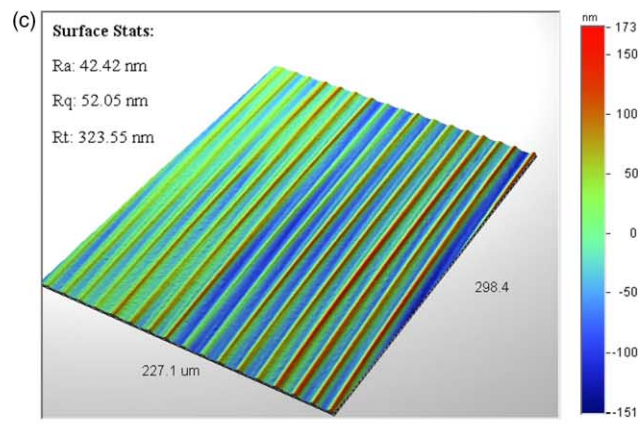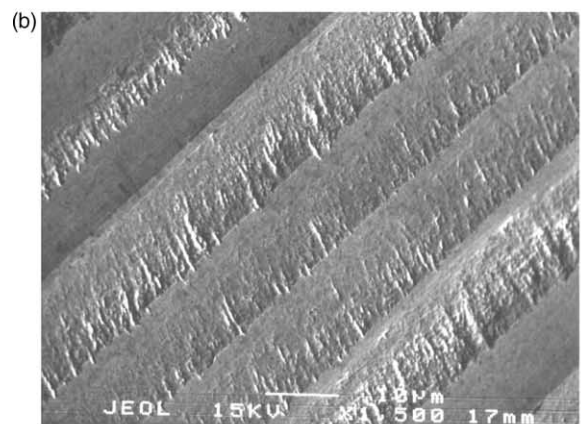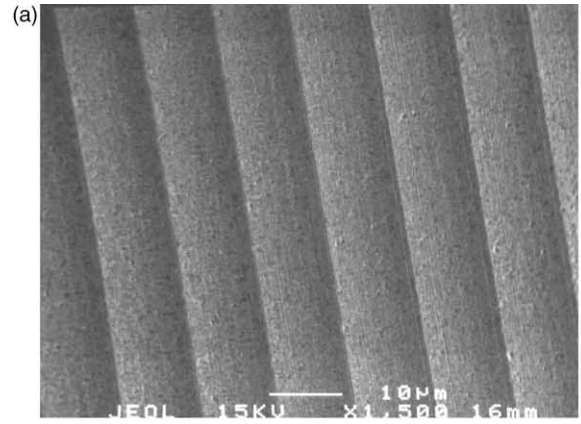

Fig. 16. (a) SEM image for <100> workpiece, <100> cutting direction, 'smooth' region. (b) Image for <100> workpiece, <110> cutting direction, 'rough' region. (c) Wyko image for <100> workpiece, <100> cutting direction, smooth region. (d) Wyko image for <100> workpiece, <110> cutting direction, 'rough' region.
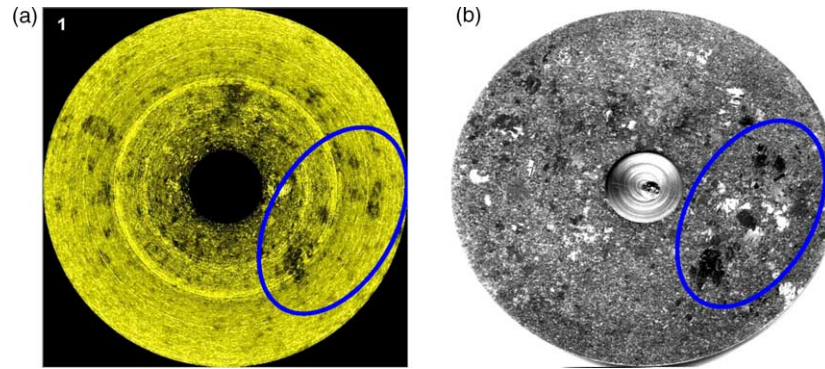
Fig. 17. (a) AE RMS polar map for polycrystalline OFHC copper workpiece. (b) Micrograph of chemically etched workpiece.

[20]. A perfectly homogenous and isotropic workpiece would most likely result in little variation in the AE signal and polar map, so variations in the AE signal can serve as useful feedback in a fully automated manufacturing environment.

8. Conclusions

As current manufacturing trends aim for smaller and finer form and features, a reliable means of process monitoring with the appropriate sensor technology is necessary to properly characterize and monitor the manufacturing operation. As demonstrated by with endpoint detection in CMP and crystallographic orientation detection in ultraprecision machining, AE is capable of meeting these requirements, especially for material removal process parameters such as material removal rates and very small uncut chip thicknesses. The use of AE as an in situ process monitoring and characterization tool can serve as a means of closely linking the manufacturing and quality control stages together, and with further development, in a fully automated manufacturing environment, the quality control stage can be entirely eliminated with optimal in situ monitoring and process control.

References

[1] N. Taniguchi, Current status in, and future trends of, ultraprecision machining and ultrafine materials processing, Annals of the CIRP 32 (1983) 2.

[2] D.A. Dornfeld, Y. Lee, A. Chang, Monitoring of ultraprecision machining processes, International Journal of Advanced Manufacturing Technology 21 (2003) 571–578.

[3] T. Moriwaki, Experimental analysis of ultra-precision machining, International Japan Society of Precision Engineering 29 (4) (1995) 287–290.

[4] Y. Lee, Monitoring and planning for open architecture manufacturing of precision machining using acoustic emission, PhD Dissertation, Mechanical Engineering Department, University of California at Berkeley, 1991.

[5] D.A. Dornfeld, W. Konig, G. Kettler, Present state of tool and process monitoring in cutting, Proceedings of New Developments in Cutting, VDI Berichte NR 988, Dusseldorf, 1993 pp. 363–376.

[6] J. Tlusty, G.C. Andrews, A critical review of sensors for unmanned machining, CIRP Annals 32 (2) (1983).

[7] H.K. Tonshoff, J.P. Wulfberg, H.J.J. Kals, W. Konig, Developments and trends in monitoring and control of machining processes, CIRP Annals 37 (2) (1988).

[8] G. Byrne, D.A. Dornfeld, I. Inasaki, W. Konig, R. Teti, Tool condition monitoring (TCM)—the status of research and industrial application, CIRP Annals 44 (2) (1995).

[9] K. Iwata, Sensing technologies for improving the machine tool function, Proceedings of the Third International Machine Tool Engineer's Conference, JMTBA, Tokyo, 1988, pp. 87–109.

[10] R.M. Fisher, J.S. Lally, Microplasticity detected by an acoustic technique, Canadian Journal of Physics 45 (1967) 1147.

[11] T. Moriwaki, Application of acoustic emission measurement to sensing of wear and breakage of cutting tool, Bulletin Japan Society of Precision Engineering 17 (1983) 154–160.

[12] J.J. Liu, Monitoring the precision machining process: sensors, signal processing, and information analysis, PhD Dissertation, Mechanical Engineering Department, University of California at Berkeley, 1991.

[13] X. Chen, J. Tang, D.A. Dornfeld, Monitoring and analysis of ultraprecision metal cutting with acoustic emission, Mechanical Engineering Congress and Exposition, ASME, Atlanta, GA, 1996, p. 387.

[14] J.F.G. Oliveira, D.A. Dornfeld, Application of AE contact sensing in reliable grinding monitoring, CIRP Annals 50 (1) (2001).

[15] E.N. Diei, D.A. Dornfeld, A model of tool fracture generated acoustic emission during machining, ASME Transactions Journal of Engineering Industry 109 (3) (1987) 227–234 also appears in Sensors and Controls for Manufacturing, E. Kannatey-Asibu and A.G. Ulsoy (Eds.), ASME, New York, 1985..

[16] E.N. Diei, D.A. Dornfeld, Acoustic emission from the face milling Process—the effects of process variables, ASME Transactions Journal of Engineering Industry 109 (2) (1987) 92–99.

[17] J. Ansenk, N. Broens, Investigation on acoustic emission mapping applications in milling, OPF Report, University of Sao Paulo, Sao Carlos, Brazil, 2004.

[18] R. DeJule, CMP challenges below a quarter micron, Semiconductor International (1997) 54–60.

[19] I. Hwang, In-situ process monitoring and orientation effects-based pattern design for chemical mechanical planarization, PhD Dissertation, Mechanical Engineering Department, University of California at Berkeley, 2004.

[20] D.A. Dornfeld, J.F.G. Oliveira, D. Lee, C.M.O. Valente, Analysis of tool and workpiece interaction in diamond turning using graphical analysis of acoustic emission, CIRP Annals 52 (1) (2003).